Journal of Materials Chemistry A

PAPER

View Article Online
View Journal | View Issue

Check for updates

Cite this: J. Mater. Chem. A, 2019, 7, 19081

Core–shell TiO_2@C ultralong nanotubes with enhanced adsorption of antibiotics†

Zhe Wang,[a] Hongmei Tang,[a] Wenyao Li, *[ab] Jianwei Li,[c] Ruoyu Xu,[b] Kenan Zhang,[a] Guanjie He, *[bc] Paul R. Shearing [b] and Dan J. L. Brett *[b]

Received 22nd June 2019
Accepted 18th July 2019

DOI: 10.1039/c9ta06735c

rsc.li/materials-a

As materials capable of adsorbing antibiotics continue to be developed, composite adsorbents have been shown to offer advantages over mono-material adsorbents. In this work, ultralong titanium dioxide@carbon nanotubes were prepared by a simple hydrothermal treatment, followed by carbonization. The composite material is able to adsorb three different categories of antibiotics, including tetracycline (TC), ofloxacin (OFO) and norfloxacin (NFO). The adsorption results show that the adsorption properties of composite materials have been greatly improved compared with single inorganic adsorbent materials, for which the adsorption capacities are 240 mg g^{-1} (TC), 232 mg g^{-1} (OFO), and 190 mg g^{-1} (NFO), respectively. The adsorption mechanism is consistent with a Langmuir pseudo-first-order kinetic model.

Open Access Article. Published on 24 julio 2019. Downloaded on 18/07/2025 21:58:29.
This article is licensed under a Creative Commons Attribution 3.0 Unported Licence.

Introduction

With the discovery of antibiotics, such as penicillin, for human beings to fight infectious diseases, there is a common phenomenon of abusing antibiotics to cope with various illnesses.[1] However, antibiotics are difficult to metabolize in a short period of time in animals, plants and humans. Simultaneously, emissions from pharmaceutical companies have also caused enormous environmental pollution.[2,3] Thus, a large amount of used antibiotics went to the soils, rivers, animals, *etc.* The accumulation of these residual antibiotics not only pollutes the environment, but also causes harm to human health.[4] With the emergence of super bacteria, there is serious concern that society will lack the required antibiotics in future.[5] The warnings of scientists have attracted the attention of the public and governments. Therefore, searching for effective and non-toxic methods to remove antibiotic pollutants has become a hot research topic.

There are a number of methods which aim to decrease the amount of antibiotics in the environment, including adsorption,[6] photocatalysis,[7] electrochemical oxidation,[8] advanced oxidation[9] and biodegradation.[10] Among these methods, adsorption is a simple and cheap way to solve the problem of antibiotic pollution and can be divided into two categories: chemisorption and physisorption. Chemisorption requires high activation energy and usually higher temperatures, while physisorption is usually caused by molecular force and can occur at lower temperature. Furthermore, the chemisorption reaction may be undetectable at low temperature or pressure.[11] As characteristic of physisorption, for gases at temperatures above their critical temperature, adsorption is confined to a monolayer (unimolecular).[12] Therefore, the adsorption capacity is related to the specific surface area and structures of the adsorbents. The effects of the specific surface area and structure of different types of single adsorbent materials and composite adsorbent materials on the adsorption capacity have been studied in depth.[13] Promising materials, such as zeolites for adsorption of tetracycline,[14] attapulgite/carbon composites for adsorption of tetracycline,[15] and oil shale powders[16] and functional MOFs for adsorption of norfloxacin,[17] were reported. A large number of experimental results show that the specific surface area and the structure of composites are the key factors that make adsorption more effective than with a single material. Therefore, there is an increasing focus on developing composite adsorbent materials with an optimized structure and high specific surface area *via* simple preparation processes amenable to mass production.

In this work, ultralong TiO_2 nanotubes were prepared using a simple hydrothermal treatment. In order to sustain the ultralong structure and increase the specific surface area, the ultralong TiO_2 nanotubes were covered with an ultrathin carbon layer by carbonizing ethanol, and thus a core–shell TiO_2@C ultralong nanotube composite was formed. Three common antibiotics, *i.e.*, tetracycline (TC), ofloxacin (OFO) and norfloxacin (NFO), were adsorbed by the TiO_2@C composite, and the adsorption capacities were measured to be 240 mg g^{-1}, 232 mg g^{-1}, 190 mg g^{-1}, respectively, which are higher than those of many of the reported single and composite adsorbent materials. Therefore, the core–shell TiO_2@C nanotubes are promising adsorbent materials for antibiotic pollutants. This

[a]School of Material Engineering, Shanghai University of Engineering Science, Shanghai 201620, China. E-mail: liwenyao314@gmail.com

[b]Electrochemical Innovation Lab, Department of Chemical Engineering, University College London, London WC1E 7JE, UK. E-mail: d.brett@ucl.ac.uk

[c]Department of Chemistry, University College London, London, WC1H 0AJ, UK. E-mail: g.he@ucl.ac.uk

† Electronic supplementary information (ESI) available. See DOI: 10.1039/c9ta06735c

Open Access Article. Published on 24 julio 2019. Downloaded on 18/07/2025 21:58:29.
This article is licensed under a Creative Commons Attribution 3.0 Unported Licence.

study sheds light on the mechanism of metal oxide/carbon hybrids for adsorbing antibiotics and identifies routes to improve performance.

Experimental section

Preparation of ultralong titanium dioxide nanotubes

Firstly, 0.5 g P_{25} (a commercial titanium dioxide which is an anatase and rutile two-phase mixture nanopowder with an average particle diameter of 25 nm) was added into 40 mL of 10 mol L^{-1} NaOH solution and dispersed in a 50 mL reaction kettle, which was ultrasonicated for 5 min to obtain a homogeneous solution. The reaction kettle was sealed and put into an oil bath at 120 °C for 48 h with magnetic stirring (Fig. 1a). When the reaction finished, the reactor was taken out and cooled to room temperature. The obtained white products were washed with 0.1 mol L^{-1} HNO_3 and centrifuged several times until the pH reached 7. The final products were washed with deionized water and placed in a vacuum drying oven at 60 °C for 8 h.

Preparation of TiO_2@C core–shell structures

The as-prepared products were placed in the middle of a tube furnace, N_2 gas was purged through anhydrous ethanol and then into the tube furnace, and the reaction temperature was set at 400 °C for 10 h under a nitrogen atmosphere. Black products (TiO_2@C composite) were obtained as the reaction finished. The experimental schematic diagram is shown in Fig. 1b.

Characterization

The prepared TiO_2@C composites were characterized by scanning electron microscopy (SEM, S-4800, Japan) and transmission electron microscopy (TEM, JEM-2100F, Japan). The crystal structure and components of the material were determined using an X-ray diffractometer (XRD, Rigaku, Cu-Kα radiation, Japan). The specific surface area and the pore size distribution of the material were determined from the Brunauer–Emmett–Teller (BET) test (ASAP 2020, Micromeritics, America). The surface chemical structure was determined by Fourier transform infrared spectroscopy (FT-IR) (6700, Nicolet, USA) and Raman spectroscopy (Lab RAM, HR800) with 532 nm laser light. The absorbance of the TiO_2@C composite materials was measured using a UV spectrophotometer (G-9, Rangqi, China). The functional groups and the elemental states on the surface of the adsorbents were examined by X-ray photoelectron spectroscopy (XPS) analysis, which was conducted on a Kratos Axis Ultra DLD spectrometer, using monochromated Al Kα X-rays at a base pressure of 1×10^{-9} Torr.

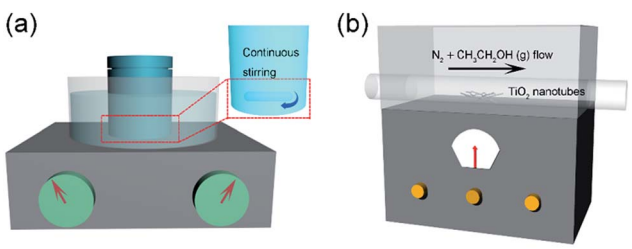

Fig. 1 Schematic of the preparation process for TiO_2@C.

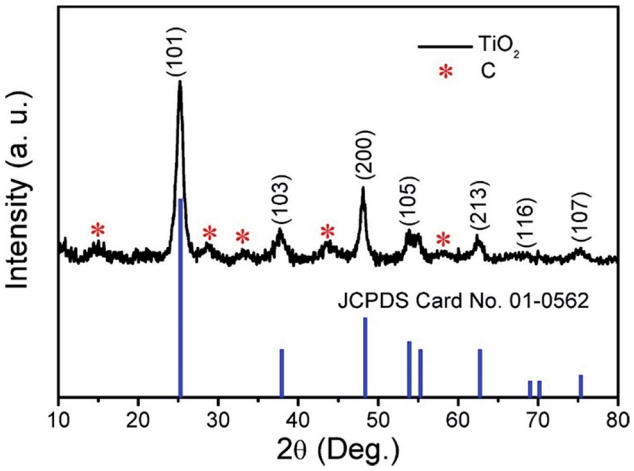

Fig. 2 XRD pattern of the obtained products.

Results and discussion

The result of XRD analysis is shown in Fig. 2; the main diffraction peaks could be indexed to the (101), (103), (200), (105), (213), (116) and (107) reflections, corresponding to anatase phase TiO_2 with the JCPDS card no. 01-0562. The result also confirms that C exists in the TiO_2 products (marked with red asterisks). The C species were further tested by Raman spectroscopy and the result is shown in Fig. S1.† The peak intensity ratio between the G band and D band (I_G/I_D) is 1.1796, indicating that the proportion of carbon defect structures in the carbon structure is relatively small and the dominant component in the carbon structures is the sp^2.

The low- and high-magnification SEM images of the TiO_2@C products are shown in Fig. 3a and b. From the SEM images, it

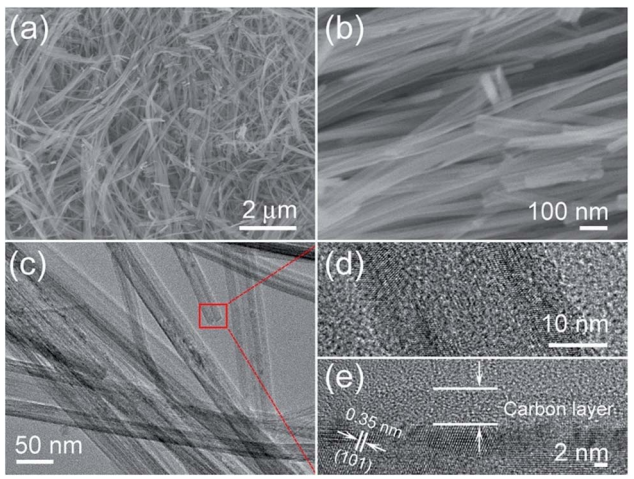

Fig. 3 Microstructure characterization of the core–shell TiO_2@C nanotubes: (a and b) low and high-magnification SEM images, and (c) TEM and (d and e) HRTEM images.

This journal is © The Royal Society of Chemistry 2019

Open Access Article. Published on 24 julio 2019. Downloaded on 18/07/2025 21:58:29.
This article is licensed under a Creative Commons Attribution 3.0 Unported Licence.

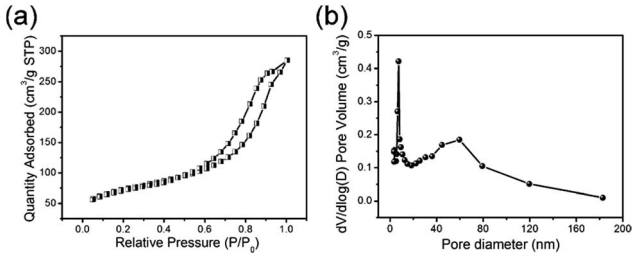

Fig. 4 (a) The N_2 adsorption–desorption isotherm and (b) pore diameter distribution of the TiO_2@C nanotubes.

can be seen that the length of the TiO_2@C nanotubes can be up to several micrometers, representing an 'ultralong' structure. From the TEM image of Fig. 3c, it can be confirmed that the composite material is a tubular nanostructure. More detailed information on the material can be obtained from Fig. 3d; the outer diameter of the nanotubes is ~35 nm, and the inner diameter is ~15 nm, and the thickness of the carbon layer is 5–6 nm (Fig. 3e). This shows that the carbon layer was successfully coated on the outside of the TiO_2 nanotubes, and the interplanar spacing of 0.35 nm indicates the (101) lattice plane of the TiO_2 crystal.

The detailed specific surface area of the TiO_2@C core–shell nanotubes can be obtained from the N_2 adsorption–desorption curve (Fig. 4a). The specific surface area of TiO_2@C can be calculated from the N_2 adsorption–desorption isotherm, and the BET value is 346.26 $m^2\ g^{-1}$, which is higher than that of the single TiO_2 (Fig. S2 in the ESI†). Fig. 4b shows the pore size distribution of the TiO_2@C nanotubes, with a main diameter of around 15 nm, which corresponds to the diameter of the nanotubes. The diameter of ~60 nm can be attributed to the gaps between the nanotubes.

The adsorption of the three kinds of antibiotics is based on the classical monolayer Langmuir model and the multilayer Freundlich adsorption model. The Langmuir equation depicts

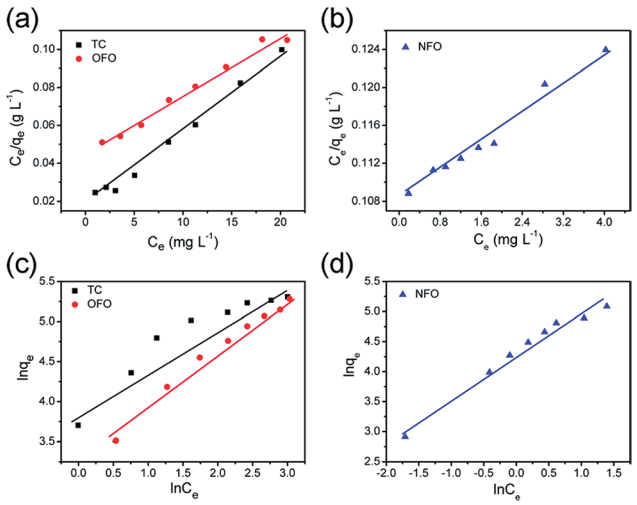

Fig. 5 The liner fitting curves of the Langmuir (a and b) and Freundlich (c and d) models for TiO_2@C towards NFO, TC and OFO.

Table 1 Langmuir and Freundlich regression data from the adsorption isotherms of NFO, TC and OFO for the TiO_2@C

Pollutant	Langmuir K_L (L mg^{-1})	Langmuir q_m (mg g^{-1})	Langmuir R^2	Freundlich k_f	Freundlich n	Freundlich R^2
NFO	0.0488	190	0.979	70.8014	1.4105	0.940
TC	0.2562	240	0.989	53.4171	1.9861	0.874
OFO	0.0963	232	0.980	26.0860	1.4714	0.960

the process of randomly adsorbing species onto the surface of the adsorbent. The linearization equation of the Langmuir adsorption model is shown as follows:[18]

$$\frac{c_e}{q_e} = \frac{1}{K_L q_m} + \frac{c_e}{q_m} \quad (1)$$

where C_e is the balance concentration (mg L^{-1}), K_L is the adsorption constant (L mg^{-1}), q_m is the maximum adsorption capacity (mg g^{-1}), and q_e represents the quantity (mg g^{-1}) of antibiotics adsorbed at equilibrium.

The Freundlich adsorption model is an empirical equation that is simple and widely used. It can simulate a multi-layer adsorption process, which means that the adsorption sites on the adsorption surface are not uniform. The linearized form of the Freundlich adsorption model equation is as follows:[19]

$$\ln q_e = \ln K_f + \left(\frac{1}{n}\right) \ln C_e \quad (2)$$

where K_F and n represent the Freundlich constant [(mg g^{-1}) (L $mg^{-1})^{1/n}$] and adsorption intensity of the adsorbents, respectively.[20–22] The mass of the TiO_2@C materials used in this study was 5 mg, for adsorption of 5–40 mg L^{-1} tetracycline (TC), 5–40 mL ofloxacin (OFO) and 2–20 mg L^{-1} norfloxacin (NFO). Adsorption equilibrium was achieved after magnetic stirring at room temperature. Fig. 4 shows the experimental data of the TiO_2@C nanotubes adsorbing the three kinds of antibiotics: OFO, TC and NFO. Fig. 5a and b are the Langmuir model fitting charts, and Fig. 5c and d show the corresponding Freundlich model fitting charts. The fitting data are shown in Table 1. From the correlation coefficient (R^2) value of the two models, it can be concluded that the three kinds of antibiotics adsorbed by the material are more consistent with the Langmuir model. The maximum adsorption capacities of OFO, TC and NFO, calculated using the Langmuir model, are 232 mg g^{-1}, 240 mg g^{-1}, and 190 mg g^{-1}, respectively. The experimental results show that the adsorption amount of this material is greatly improved compared with other inorganic materials, as shown in Table 2.

Adsorption kinetic model

The adsorption kinetics of the three kinds of antibiotics were studied. The pseudo-first-order model was based on the assumption that the adsorption was controlled by diffusion.[29] The pseudo-first-order dynamic model is as follows:[30]

$$\ln(q_e - q_t) = \ln q_e - K_1 t \quad (3)$$

Open Access Article. Published on 24 julio 2019. Downloaded on 18/07/2025 21:58:29.
This article is licensed under a Creative Commons Attribution 3.0 Unported Licence.

Table 2 The adsorption capacity comparison of the adsorbent materials

Antibiotics	Adsorbents	q_m (mg g^{-1})	Conditions	Ref.
Tetracycline	Zeolite	130	pH = 7	14
	GSO	137	pH = 7	23
	PS/GO	197.9	pH = 6	24
	PC@CMCS	136.9	pH = 7	25
	Ultralong hydrogen titanate nanobelts	151.51	PH = 7	26
	TiO_2@C	240	pH = 7	This work
Norfloxacin	AMPH	1.42	pH = 7	27
	MIP	29.35	pH = 8	28
	Ultralong hydrogen titanate nanobelts	111.73	pH = 7	26
	TiO_2@C	190	pH = 7	This work
Ofloxacin	Oil shale powders	15.4	pH = 7.5	16
	Ultralong hydrogen titanate nanobelts	148.14	pH = 7	26
	TiO_2@C	232	pH = 7	This work

The pseudo-second-order kinetic model assumes that the adsorption rate is determined by the square value of the number of adsorbed vacancies on the surface of the adsorbent. The pseudo-second-order dynamic model is as follows:[31]

$$\frac{t}{q_t} = \frac{1}{K_2 q_e^2} + \frac{t}{q_e} \quad (4)$$

where q_e is the concentration of adsorption at equilibrium (mg g^{-1}), q_t is the amount of adsorption (mg g^{-1}) at time t, K_1 is the pseudo-first-order adsorption rate constant, and K_2 is the pseudo-second-order adsorption rate constant.[17] The fitting data of the dynamics of the three kinds of antibiotics are given in Table 3.

Fig. 6 shows the pseudo-first-order and pseudo-second-order kinetic models of the three antibiotics, and the intra-particle-diffusion model. As Table 3 shows, the pseudo-first-order model best describes the adsorption mechanism. Thus, the adsorption process of TiO_2@C adsorbing OFO, TC and NFO is mainly controlled by diffusion.[32] In order to obtain more information on the adsorption process, data are fitted to the intra-particle-diffusion model, as follows:[33]

$$q_t = K_{id} t^{1/2} + C \quad (5)$$

Adsorption can be divided into two processes: adsorbent surface adsorption and slow pore diffusion. The particle diffusion model is the most suitable for describing the dynamics of particles in the particle diffusion process.[34] The linear fitting of q_t and $t^{1/2}$ gives a straight line that passes through the origin and shows that particle diffusion is the rate determining step.[35] From Fig. 6c, it can be seen that the TiO_2@C particle diffusion model is divided into three stages; the first phase is the diffusion of the boundary layer, which is mainly the external mass transfer of the adsorbent. The second phase refers to the internal diffusion of particles, which is mainly the transport of microstructures of adsorbents, such as holes. These two stages make up the intra-particle diffusion model. Because the contact angle between the material itself and the solution is different, the time needed for different materials to reach adsorption equilibrium is different. The third phase is usually not considered as a rate-controlling step, generally referring to the procession of adsorption being close to adsorption equilibrium, which means that the active sites of the internal and external surfaces are mostly occupied. Compared with single titanium dioxide nanotube materials, the contact angle of the composites changed due to the synergistic effect of titanium dioxide nanotubes and the carbon layer, which greatly improved the adsorption performance of the material[36] (Fig. S3†).

In order to understand the change that has occurred on the surface of the TiO_2 nanotubes, FTIR and XPS tests were carried out and TC was selected as an example. Fig. 7a shows the FTIR comparison, before and after the adsorption of TC. The

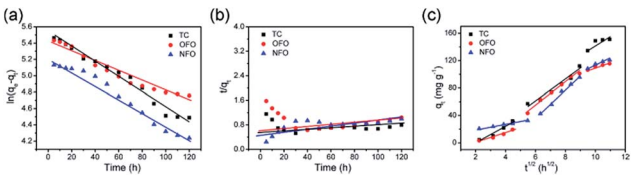

Fig. 6 (a) The pseudo-first-order model of OFO, TC, and NFO, (b) the pseudo-second-order model of OFO, TC, and NFO, and (c) the intra-particle-diffusion model of OFO, TC, and NFO.

Table 3 OFO, TC and NFO dynamic correlation fitting data

Model	C_0	Pseudo-first-order, K_1	$q_{e,cal.}$	R^2	Pseudo-second-order, K_2	$q_{e,cal.}$	R^2
OFO	40	0.00647	230.2	0.95	7.32×10^{-6}	769.2	0.52
TC	40	0.00909	252.1	0.97	2.84×10^{-6}	454.5	0.50
NFO	20	0.00874	191.2	0.97	2.99×10^{-5}	248.7	0.47

This journal is © The Royal Society of Chemistry 2019

Open Access Article. Published on 24 julio 2019. Downloaded on 18/07/2025 21:58:29.
This article is licensed under a Creative Commons Attribution 3.0 Unported Licence.

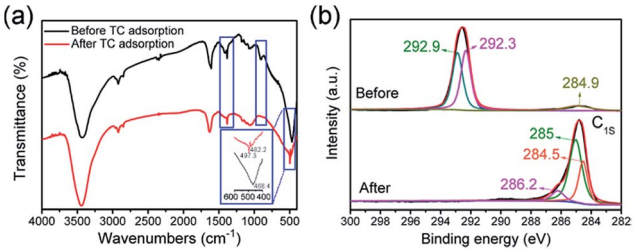

Fig. 7 (a) The FTIR spectra of TiO_2@C before and after adsorbing TC, (b) high-resolution XPS spectra of the C 1s peaks before and after adsorption of the TC antibiotic by TiO_2@C.

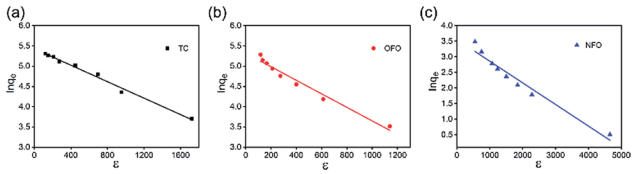

Fig. 8 (a–c) D–R isotherm regression fitting lines from the adsorption isotherms of TC, OFO and NFO for the TiO_2@C.

absorption peak at 2920 cm^{-1} is attributed to the C–H bond. The hydrogen ion was introduced into the soaking TiO_2 nanotubes from dilute nitric acid, combined with a small amount of carbon into the C–H bond. The absorption peak at 1384 cm^{-1} is the result of the N–O bond introduced by TiO_2 nanotubes with dilute nitric acid.[5] The smaller absorption peaks at 1066 cm^{-1} and 903 cm^{-1} are due to the telescopic vibration of the C–O bond. The absorption peak of TiO_2@C at 1609 cm^{-1} is the characteristic peak of the amide group. After adsorption of TC, the peak shifted to 1630 cm^{-1}, indicating that TC was successfully adsorbed on TiO_2@C. The sharp peak at 468 cm^{-1} is the result of the vibration of the Ti–O bond of titanium dioxide nanotubes. In addition, the carbonyl group is formed by the combination of some oxygen elements, which makes the Ti–O bond peak of the TiO_2@C composite blunt and the peak shifts to 497 cm^{-1}. The analysis of FT-IR results showed that the adsorption of TiO_2@C on TC was mainly physical adsorption, which was in accordance with the pseudo-first-order kinetic model. To further prove that TC has been adsorbed by TiO_2@C, XPS spectra (Fig. S4†) of the C 1s peaks of adsorbents before and after adsorption are compared. After deconvolution, the C 1s signal can be separated into a C=C/C–C peak at 284.9 eV, a C–O peak at 292.3 eV and a C=O peak at 292.9 eV (Fig. 8b). It is noted that the content of C=C/C–C is much lower than that of C=O. However, after the TC antibiotic was adsorbed by TiO_2@C, the adsorbed C 1s signal is deconvoluted to a C=C/C–C peak at 284.5 eV, a C–O peak at 285 eV and a C=O peak at 286.2 eV. Simultaneously, the content of C–C/C=C increased sharply. In contrast, the content of C=O is the lowest among the three kinds of chemical bonds. In summary, the increase of C=C/C–C is due to the benzene ring of TC. When the TC antibiotic was adsorbed by TiO_2@C, the C=O would be replaced by C=C/C–C. Thus, it is noted from the XPS spectra that the TC antibiotic can be adsorbed by TiO_2@C effectively.

Table 4 D–R equation regression data from the adsorption isotherms of NFO, TC and OFO for the TiO_2@C

Pollutant	B_D ($mol^2\ J^{-2}$)	D–R equation q_m(mmol g^{-1})	R^2	E (KJ mol^{-1})
TC	1.01×10^{-3}	225.88	0.983	0.700
OFO	1.67×10^{-3}	202.35	0.966	0.423
NFO	6.90×10^{-4}	35.59	0.953	1.025

Table 5 The values of ΔG calculated for adsorption of the three antibiotics by TiO_2@C

Pollutant (40 mg L^{-1})	TC	OFO	NFO
ΔG (kJ mol^{-1})	−5.71	−5.58	−5.172

The D–R isotherm model can be applied to identify the type of adsorption, *i.e.*, physical or chemical adsorption process. The linear D–R isotherm[37] models are as follow and the results are shown in Fig. 8:

$$\mathrm{In}\ q_e = \mathrm{In}\ q_m - B_D\varepsilon \quad (6)$$

$$\varepsilon = RT\ \mathrm{In}(1 + 1/C_e) \quad (7)$$

where q_e and q_m (mmol g^{-1}) are the equilibrium antibiotics solution concentration on the adsorbent and maximum adsorption capacity, respectively, B_D is a constant related to the adsorption energy ($mol^2\ J^{-2}$), ε is the Polanyi potential, C_e is the equilibrium concentration (mol L^{-1}), R is the gas constant and T is the absolute temperature (K).

The adsorption free energy (E) can be calculated according to Polanyi potential from the following equation:

$$E = 1/\sqrt{2} \times B_D \quad (8)$$

Compared with the value of R^2, it is obvious that the Langmuir model is more fit for the experimental data. As for the D–R equations, if the value of E is less than 8 kJ mol^{-1}, physical sorption is considered as the main mechanism, while chemical sorption will be expected if the value of E is in the range of 8–16 kJ mol^{-1}. As shown in Table 4, the three values of E are all less than 8 kJ mol^{-1}. This proves that physisorption is the main sorption mechanism. The results of this analysis yielded consistent pseudo-first-order adsorption kinetics.

The thermodynamics parameters regarding antibiotic adsorption onto TiO@C, such as Gibbs free energy (ΔG), and the solid and liquid phases at equilibrium (K_d), can be calculated using the following equations:[38]

$$K_d = q_e/c_e \quad (9)$$

$$\Delta G = -R\ \mathrm{In}(K_d) \quad (10)$$

Generally, if $-20 < \Delta G < 0$ kJ mol^{-1}, physical adsorption is dominant and it changes to more negative values than

Open Access Article. Published on 24 julio 2019. Downloaded on 18/07/2025 21:58:29.
This article is licensed under a Creative Commons Attribution 3.0 Unported Licence.

-40 kJ mol^{-1} for chemical adsorption. As shown in Table 5, the calculated result is consistent with D–R equations and pseudo-first-order adsorption kinetics.

Conclusions

Core–shell TiO_2@C ultralong nanotubes were prepared using a solvothermal process followed by anhydrous ethanol carbonization. The TiO_2@C exhibits a mesoporous structure and large specific surface area. The adsorption experiment proves that the TiO_2@C composite adsorbent can adsorb three kinds of typical antibiotics (TC, OFO, and NFO) effectively. Moreover, the main determinant of the adsorption process is proved to be physical adsorption rather than chemical adsorption, and the adsorption process fits the Langmuir and pseudo-first-order models. Therefore, the work provides a practical case for the future development of more composite adsorbents and lays a foundation for the industrialization of composite materials.

Conflicts of interest

There are no conflicts to declare.

Acknowledgements

The work has been funded by the National Natural Science Foundation of China (51602193, 21601122, and 51701022), the Shanghai "Chen Guang" Project (16CG63), the Fundamental Research Funds for the Central Universities (WD1817002), and the Talent Program of Shanghai University of Engineering Science, Science and Technology Facilities Council for STFC/MDC Futures Early Career Award.

References

1 E. A. Abdullah, A. H. Abdullah, Z. Zainal, M. Z. Hussein and T. K. Ban, *J. Environ. Sci.*, 2012, **24**(10), 1876–1884.
2 A. K. Sarmah, M. T. Meyer and A. B. Boxall, *Chemosphere*, 2006, **65**, 725–759.
3 M. Saravanana, J. H. Hur, N. Arul and M. Ramesh, *Environ. Toxicol. Pharmacol.*, 2014, **38**, 948–958.
4 H. A. Al-Aoh, R. Yahya, M. Jamil Maah and B. A. M. Radzi, *Desalin. Water Treat.*, 2014, **52**(34–36), 6720–6732.
5 S. Rodriguez-Mozaz, S. Chamorro, E. Marti, B. Huerta, M. Gros, A. Sànchez-Melsió, C. M. Borrego, D. Barcelo and J. L. Balcazar, *Water Res.*, 2015, **69**, 234–242.
6 T. T. Lu, Y. F. Zhu, Y. X. Qi, W. B. Wang and A. Q. Wang, *Int. J. Biol. Macromol.*, 2018, **106**, 870–877.
7 F. Bianculloa, N. F. F. Moreiraa, A. R. Ribeiroa, C. M. Manaia, J. L. Faria, O. C. Nunes, S. M. Castro-Silva and A. M. R. Silva, *J. Chem. Eng.*, 2019, **367**, 304–313.
8 H. Yu, B. X. Zhang, M. Zhao, L. Zhang, H. Dong and H. B. Yu, *Catal. Today*, 2019, **327**, 308–314.
9 J. C. Espíndola, K. Szymanski, R. O. Cristovao, A. Mendes, V. J. P. Vilara and S. Moziab, *Catal. Today*, 2019, **328**, 274–280.
10 C. L. Amorim, I. S. Moreira, A. S. Maia, M. E. Tiritan and P. M. Castro, *Appl. Microbiol. Biotechnol.*, 2014, **98**, 3181–3190.
11 R. Françoise, R. Jean and S. Kenneth, *Adsorption by Powders and Porous Solids*,1999, pp. 1–26.
12 E. Can, *Supercritical Fluid Science & Technology*,2011, vol. 1, pp. 41–77.
13 D. D. Wang, Y. L. Shen, Y. L. Chen, L. L. Liu and Y. F. Zhao, *J. Chem. Eng.*, 2019, **367**, 260–268.
14 H. Huang, Y. L. Zou and Y. N. Li, *Adv. Mater. Res.*, 2012, **512–515**, 2355–2360.
15 J. Tang, L. Zong, B. Mu, Y. R. Kang and A. Q. Wang, *Korean J. Chem. Eng.*, 2018, **35**, 1650–1661.
16 A. Gouza, S. Saoiabi, M. El Karbane, S. Masse, G. Laurent, A. Rami, A. Saoiabi, A. Laghzizil and T. Coradin, *Environ. Sci. Pollut. Res.*, 2017, **24**(33), 25977–25985.
17 Y. Zhuang, F. Yu, J. Ma and J. H. Chen, *Desalin. Water Treat.*, 2016, **57**(20), 9510–9519.
18 P. K. Baskaran, B. R. Venkatraman and S. Arivoli, *Eur. J. Chem.*, 2011, **8**(1), 9–18.
19 A. H. Ali, *Desalin. Water Treat.*, 2013, **51**(28–30), 5547–5558.
20 L. Yu, X. Liu, W. Yuan, L. J. Brown and D. Wang, *Langmuir*, 2015, **31**, 6351–6366.
21 S. K. Singh, T. G. Townsend, D. Mazyck and T. H. Boyer, *Water Res.*, 2012, **46**, 491–499.
22 M. Iram, C. Guo, Y. Guan, A. Ishfaq and H. Z. Liu, *J. Hazard. Mater.*, 2010, **181**, 1039–1050.
23 Y. Zhuang, F. Yu, J. Ma and J. H. Chen, *Desalin. Water Treat.*, 2016, **57**(20), 9510–9519.
24 L. C. Chen, S. Lei, M. Z. Wang, J. Yang and X. W. Ge, *Chin. Chem. Lett.*, 2016, **27**(4), 511–517.
25 J. S. He, J. D. Dai, A. T. Xie, S. J. Tian, Z. S. Chang, Y. S. Yan and P. W. Huo, *RSC Adv.*, 2016, **6**(87), 84536–84546.
26 W. Y. Li, J. R. Wang, G. J. He, L. Yu, N. Noor, Y. G. Sun, X. Y. Zhou, J. Q. Hu and I. P. Parkin, *J. Mater. Chem. A*, 2017, **5**(9), 4352–4358.
27 R. A. Wuana, R. Sha'Ato and S. Iorhen, *Desalin. Water Treat.*, 2016, **57**(25), 11904–11916.
28 Y. Kong, N. W. Wang, X. N. Ni, Q. Y. Yu, H. Liu, W. H. Huang and W. Z. Xu, *J. Appl. Polym. Sci.*, 2016, **133**(1), 42817.
29 L. Zhang, H. A. Loaiciga, M. Xu, C. Du and Y. Du, *Int. J. Environ. Res. Public Health*, 2015, **12**(11), 14312–14326.
30 D. Feng, H. M. Yu, H. Deng, F. Z. Li and C. J. Ge, *BioResources*, 2015, **10**(4), 6751–6768.
31 M. A. Al-Anber, *Desalin. Water Treat.*, 2014, **52**(13–15), 2560–2571.
32 N. A. Rashidi, S. Yusup, A. Borhan and L. H. Loong, *Clean Technol. Environ. Policy*, 2014, **16**(7), 1353–1361.
33 X. Y. Cao, H. L. Pang and G. P. Yang, *J. Soils Sediments*, 2015, **15**(7), 1635–1643.
34 A. R. Kul and H. Koyuncu, *J. Hazard. Mater.*, 2010, **179**(1–3), 332–339.
35 Q. Liu, Q. Z. Liu, W. Ma, W. L. Liu, X. X. Cai and J. S. Yao, *Colloids Surf., A*, 2016, **511**, 8–16.
36 L. L. Jia, X. Y. Huang, H. E. Liang and Q. Tao, *Int. J. Biol. Macromol.*, 2019, **132**, 1039–1043.
37 M. A. Barakat and R. Kumar, *J. Ind. Eng. Chem.*, 2015, **23**, 93–99.
38 O. Pezoti, A. L. Cazetta, K. C. Bedin, L. S. Souza, A. C. Martins, T. L. Silva, O. O. Santos, J. V. Visentainer and V. C. Almeida, *Chem. Eng. J.*, 2016, **288**, 778–788.

 This journal is © The Royal Society of Chemistry 2019